Supporting Information

Photonic Double-Network Hydrogel Dressings with Antibacterial Phototherapy and Inflammation Regulation for General Management of Cutaneous Regeneration

Jiyu Sun[1,2,#], Yi Deng[1,3,4,#], Qiuyang Han[1], Daichuan Ma[5], Yau Kei Chan[3], Shuai He[1], Xiong Zhou[1,6], Hao Wang[1,2], Xinliang Fu[1,2]and Xueqi Gan[1,2,]*

1 School of Chemical Engineering, West China School of Stomatology, Sichuan University, 610065, Chengdu, China

2 State Key Laboratory of Oral Diseases, National Clinical Research Center for Oral Diseases, West China Hospital of Stomatology, Sichuan University, Chengdu, 610041, China

3 Department of Mechanical Engineering, The University of Hong Kong, Hong Kong SAR, China

4 State Key Laboratory of Polymer Materials Engineering, Sichuan University, Chengdu, 610065, China

5 Analytical & Testing Center, Sichuan University, Chengdu, 610065, China

6 Department of Biomedical Engineering, City University of Hong Kong, Hong Kong 999077, China

[#]These authors contributed equally.

Corresponding Author: Xueqi Gan*

West China School of Stomatology, Sichuan University, Chengdu, 610041, China.

E-mail: xueqigan@scu.edu.cn

Experimental Section

1. Synthesis of Bi_2S_3 Nano-Urchins and Bi_2S_3@GO Nano-HJs

Bi_2S_3@GO nano-HJs were synthesized by a facile one-step hydrothermal treatment, which is elaborated in the previous literature.[1, 2] Briefly, 500 mg $Bi(NO_3)_3 \cdot 5H_2O$ (Kelong, Chengdu, China), 300 mg L-Cys (Kelong) and GO nanosheets (Tanfeng, Suzhou, China) (50 mg, 100 mg, 150 mg) were mixed in 10 mL deionized water (D.I. water). After ultrasound for 5 min, the mixture solution was transferred into a 50 mL Teflon stainless-steel autoclave and reacted at 180 °C for 24 h. After cooling to the ambient temperature, the as-prepared products were centrifuged and rinsed alternately with ethanol and D.I. water three times to remove the residual H_2S by-products. Ultimately, the products were dried at 50 ℃, which were denoted to Bi_2S_3@GO n:1. The Bi_2S_3 nano-urchins were synthesized by the identical method without GO.

2. Fabrication of KC-Agar gel and Photonic Hydrogels

0.1 g KC (Kelong) and 0.1 g agar (Kelong) were spontaneously dissolved in 5 mL D.I. water and magnetically stirred for 30 min under 100 °C to make the solution homogeneity. Afterwards, 200 μg/mL BG 20:1 nanoparticles were supplemented into the polymeric solution, and 10 wt % potassium chloride (KCl, Kelong) was used to cross-linked the first phase of KC. Then the hot mixture was rapidly transferred into a Teflon-mold (Φ8 mm × 2 mm) for shaping, and was naturally cooled to room temperature to cross-link the second phase of agar, forming Bi_2S_3@GO/KC-Agar gel, i.e. photonic hydrogels. Besides, Bi_2S_3/KC-Agar gel and GO/KC-Agar gel were also synthesized by the same experimental procedure. KC gel was prepared through dissolving 0.1 g KC into KCl (10 wt %) solution at 100 °C, followed by chilling to ambient temperature.

3. Material Characterization

FE-SEM (S-4800, Hitachi, Japan) was used to observe the morphology of nanoparticles and the cryogenically fractured DN hydrogels. TEM (Talos F200X, Thermo-Scientific, USA)

was further applied to observe the micro-structure of nano-HJs. The chemical composition and element distribution of the nano-HJs and DN hydrogels were evaluated by EDS (Aztec X-Max80, Oxford, Britain) and XPS (Escalab 250Xi, ThermoFisher Scientific, USA). The phase structure of samples was analyzed by XRD (Philips X'Pert Pro MPD, Panalytical, Holland) with the Cu target radiation (λ = 1.5444 Å) at the 2θ from 10 ° to 80 °. Raman spectrometer (DXRxi, ThermoFisher Scientific, USA) was applied to verify the presence of GO. UV-vis spectra was measured using a UV-vis spectrophotometer (UV-1800PC, Aoelab, China) ranging from 200 nm to 1000 nm.

4. Mechanical Testing

The hydrogel samples (Φ20 mm × 15mm) were detected through a universal testing machine (5967, Instron, USA) to measure the mechanical characteristics of these photonic hydrogels. The hydrogel samples were compressed at a speed of 1 mm/min at ambient condition. The compressive strength, Young's modulus, and maximum force of hydrogels at rupture were investigated.

5. Swelling Behavior

The swelling ratios of different hydrogels were measured to determine the absorption ability towards fester fluid.[2] Hydrogels were submerged in PBS supplemented with 10 % FBS (Solarbio, Beijing, China) at 37 °C for 24 h. Afterwards, hydrogels were weighed after removal of surface water, and swelling ratio was calculated with the following formula:

$$\text{Swelling ratio (\%)} = (W_1 - W_0) / W_0 \times 100\ \% \qquad (1)$$

where W_0 represented the initial weight of hydrogels before immersion, and W_1 represented the weight of the swelling hydrogels.

6. Self-Healing Capacity

To evaluate the self-healing property of Agar gel, KC-Agar gel and Bi_2S_3@GO/KC-Agar gel, we cut the disc specimens of different hydrogels into halves. Half of KC-Agar gel was doped with blue pigment and the other half was doped with green pigment (Maries, Shanghai,

China). In the same way, one of the half Bi_2S_3@GO/KC-Agar gel was doped with garcinia yellow pigment and the other half was incorporated with orange pigment for better observation. Similarly, Agar gel was colored by red pigment and blue pigment by the same method. The cut fresh surfaces with different colors were contacted together, stored at 55 °C for 2 h, and sealed in a polyethylene (PE) bag to prevent water evaporation. After healing, photos were taken to observe the healing effectiveness.

7. Photothermal Effects of Nano-HJs and Photonic Hydrogels

Upon the irradiation of 808 nm NIR laser, the photo-activated heating curve of nano-HJs was monitored using a thermal infrared camera (E6xt, FLIR, USA) in PBS. To determine the influence of the nano-HJs concentration and powder intensity on the photothermal property, 200 μg/mL of different samples (Bi_2S_3, GO, BG n:1) were exposed to the NIR laser (808 nm) irradiation with various laser power (0.5, 1, 1.5 W/cm^2) for 15 min, and BG 20:1 samples with different concentrations (20, 50, 100, 150, 200 μg/mL) were illuminated upon NIR laser (808 nm, 1.5 W/cm^2) for 15 min. Furthermore, the photothermal stability was assessed by 5 laser on/off cycles. All temperature changes were recorded every 60 s by a thermal infrared camera. The photothermal property and photothermal stability of photonic hydrogels were evaluated through the same experimental procedure.

8. Detection of ROS

The generation of $^1O_2$ were verified by using DPBF (Aladdin, Shanghai, China) as a trapping agent. The total experiment was protected from light to prevent the photolysis of DPBF. Particularly, 1.5 mL of 0.5 mg/mL DPBF solution in dimethyl sulfoxide (Kelong) was supplemented into hydrogel samples. Then, the each of the samples were exposed to NIR (808 nm, 1.5 W/cm^2) or placed in the darkness for 15 min. The absorbance of DPBF from 280 nm to 550 nm was recorded using a UV-vis spectrophotometer under different illumination time.

After KC-Agar gel and Bi_2S_3@GO/KC-Agar gel were irradiated by a NIR laser (808 nm, 1.5 W/cm^2) for 15 min, the $^1O_2$ and $\cdot O_2^-$ production were further assessed every 5 min through using ESR (JES-FA200, JEOL, Japan). 2,2,6,6-tetramethylpiperidine-1-oxyl (TEMP, Aladdin) and 5, 5-dimethyl-1-pyrrolidine N-oxide (DMPO, Dojindo, Japan) were used for trapping $^1O_2$ and $\cdot O_2^-$, respectively.

9. Evaluation of Glutathione Depletion

The consumption of GSH was tested by colorimetry to verify the oxidative stress response of materials towards bacteria. 300 μL of 8 mM GSH (Aladdin) was added in the 48-well plate containing the hydrogel samples. Then, the mixed solution was placed in the darkness for 30 min to reach absorption-desorption equilibrium. The samples were treated with 808 nm laser (1.5 W/cm^2) or maintained under the darkness for 15 min. Afterwards, we removed hydrogels from the GSH solution and then added 450 μL Tris-HCl (Solarbio) (5 mM, pH = 8) and 150 μL DTNB (Macklin, Shanghai, China) (10 mM) into the GSH solution. The mixtures were placed at 37 °C for 30 min, and then the supernatant was collected and its the optical density (OD) value was measured at 410 nm by a microplate reader (SAF-680T, China). The chemical reaction of GSH and DTNB is shown in Figure 5h. To identify the type of ROS generated by phtonic hydrogels, as previous reported, quenching agents (•OH quenched by tert-butanol (TBA), $\bullet O_2^-$ quenched by benzoquinone (BQ), surface-bound free radicals quenched by potassium iodide (KI)) were added into reaction system before illumination.[3, 4] The following equation was used to determine the loss of GSH:

$$\text{Loss of GSH (\%)} = (OD_{GSH} - OD_S) / OD_{GSH} \times 100\ \% \qquad (2)$$

where OD_S represented the OD value of various hydrogels, and OD_{GSH} represented the OD value of positive control groups.

10. *In Vitro* Antibacterial Assays

10.1. Spread-Plate Method

In vitro bacteriostatic ability of various hydrogels with/without NIR (808 nm, 1.5 W/cm^2) was measured against Gram-positive *S. aureus* and Gram-negative *E. coli* based on the spread-plate method. Typically, the bacterial suspension (500 μL, 1.5 × 10^7 CFUs/mL) was incubated with hydrogels in 48-well plate and exposed to the NIR (808 nm, 1.5 W/cm^2) laser or in the darkness for 15 min. Then, the bacterial supernatant was aspirated and diluted 1000 times with LB medium, and then 100 μL bacteria was inoculated evenly on the LB agar plate. After incubating for 24 h under 37 °C, the pictures of bacteria colonies were captured using a digital camera (5D4, Canon, Japan), and the antibacterial efficiency was calculated by the following formula:

$$\text{Antibacterial efficiency (\%)} = (N_c - N_H) / N_c \times 100\ \% \qquad (3)$$

where N_c represented CFUs of blank control without NIR, N_H represented CFUs of various hydrogel groups.

10.2. Observation of Bacterial Morphology

The morphology of bacterial incubated with hydrogels was assessed by FE-SEM. 500 μL hydrogel was fixed onto the cell slides, and these slides were incubated with bacteria suspension under NIR (808 nm, 1.5 W/cm^2) laser or in the darkness for 15 min. The residual bacteria suspension was removed and samples were fixed with glutaraldehyde (Sino-Biolgical, Beijing, China). Afterwards, the bacteria were gradiently dehydrated by incremental alcohol (30-100 %), and bacteria were dried *via* critical point drying. After coated with gold, the bacteria on hydrogels were observed using FE-SEM.

10.3. Live/Dead Staining

For Live/Dead staining, the bacteria attached onto the hydrogels treated with/without NIR laser (808 nm, 1.5 W/cm^2) were stained utilizing a Live/Dead Bacteria Viability Kit (Thermo-Fisher, USA). Afterwards, the samples were observed under a fluorescent inverted microscope (CKX53, Olympus, Japan), in which the live bacteria were stained in green by SYTO-9 dye and dead bacteria were stained in red by propidium iodide dye.

10.4. Determination of MIC and MBC values

The minimum inhibitory concentration (MIC) and the minimum bactericide concentration (MBC) values of nanoparticles in the hydrogels were measured using the broth microdilution method.[5] An equal volume of microbial suspension (1×10^8 CFU/mL, optical density of 0.1 at 625 nm read on a microplate reader following the McFarland's standard) was added into each well. The MIC was determined in MH broth using different dilutions of Bi_2S_3 concentration range of 50-6400 μg/mL. MH broth medium with only tested bacteria was taken as the positive control, and each test was carried out in three replicates. MIC and MBC were defined as previous reports[6].

11. Cytocompatibility Evaluation

11.1. Cell Cultivation and Seeding

L929 and Hacat cells were incubated in Dulbecco's modified Eagle's media (DMEM, Hyclone, USA) supplemented with 1 % penicillin-streptomycin (KeyGEN, Jiangsu, China) and 10 % FBS. Then cells were seeded onto the 48-well plate containing sterile hydrogels, and the culture media were refreshed every 2 day.

11.2. Cell Viability

The cell viability of hydrogels was evaluated through a cell counting kit (CCK-8, Beyotime, Shanghai, China) following the manufacture instructions. Briefly, the cell suspension (2×10^4 cells/well) was seeded onto the 48-well plate, and supplemented the media extracted from different hydrogels. Then, the cells treated with/without NIR laser illumination for different period of time (0, 1, 2, 5, 10, 15 min). At a specific time (1, 3, 5 day), the culture media were substituted by a working solution containing CCK-8 (30 μL) and culture media (300 μL). After 3 h of incubation, 100 μL of the working solution was extracted, and its absorbance of the working solution at 450 nm was measured using a microplate reader.

11.3. Cell Morphology and Cytoskeleton

The cells were seeded onto the cell slides containing hydrogels in a 48-well plate (2×10^4 cells/well). After cultured for 3 day, the L929 and Hacat were fixed with 2 % paraformaldehyde (Labgic, Beijing, China) for 6 h. Then gradient ethanol was utilized to dehydrate cells. Finally, the samples were dried using critical point drying, and the cell morphology was observed using FE-SEM.

Besides the cytoskeleton and cellular nuclei were photographed by CLSM (FV3000, Olympus, Japan). In brief, cells cultured with samples were stained with Fluorescein isothiocyanate-labeled phalloidin (FITC-phalloidin, Solarbio) for F-action (green) and 4',6-Diamidino-2-Phenylindole (DAPI, Solarbio) for nucleus (blue) according to manufacturer's instructions.

11.4. Migration Ability Assay

The migration ability of L929 was determined by an *in vitro* scratch assay. The extracts were prepared by submerging hydrogels (Φ20 mm × 2 mm) of each hydrogel in 5 mL DMEM. L929 were seeded in a 6-well plate at a density of 5×10^5 cells/well and placed to achieve 90 % confluence for 24 h. Then a wound gap was carefully scratched using a 200 μL sterile pipette tip at the bottom of each well, and the cells were rinsed with PBS to remove detached cells. Afterwards, cell media were changed to the extracts of different hydrogel samples. The images were taken at different times through the inverted microscope to study the wound closure rate. The scratch area was quantified by the Image J software, and the cell migration rate was acquired by the equation below:

$$\text{Cell migration rate (\%)} = (A_0 - A_t) / A_0 \times 100\ \% \qquad (4)$$

where A_0 represented the scratch area immediately after scratch procedure, and A_t represented the wound area after time "t" of sample treatment (t = 12, 24, 60 h).

12. *In Vivo* Animal Study

12.1. Establishment of the Infectious Skin Wound Model

All *in vivo* experiments and procedures were approved by and in compliance with the Animal Ethical Committee of the West China Hospital of Stomatology Sichuan University (WCHSIRB-D-2018-089). Female Balb/c mice (7 weeks, 18 - 20 g) were purchased from Byrness Weil Biotech Ltd. (China). After anesthetizing all mice *via* an intraperitoneal injection of chloral hydrate (10 wt %), two full-thickness round wounds (Φ6 mm) were constructed on the shaved dorsal region by a biopsy punch. After removal of the full-thickness skin, the wound was inoculated with the 40 μL *S. aureus* suspension (4×10^8 CFU·mL^{-1}), and then bandaged with gauze overnight to build the model of infected skin wound. The wound in the mice from the KC-Agar gel (+) group and Bi_2S_3@GO/KC-Agar gel (+) group were irradiated by an 808 nm NIR laser (1.5 W/cm^2) for 5 min. During the treatment process, the temperature changes of the wound were captured by a thermal infrared camera. Synchronously, wound exudates (20 μL) with/without treatment were collected to assess the severity of wound infection. On the 6th day, the skin tissues on the dorsal region and major organs including the heart, liver, spleen, lung, and kidney were harvested for observation. Meanwhile, the blood of mice in all groups were drawn for CBC.

12.2. Wound Healing Assessment

Images of wound areas were captured every day for 6 days post-operation to track the development of wound regeneration by a digital camera. The wound healing rate was calculated as follows:

$$\text{Wound contraction (\%)} = (A_0 - A_n) / A_0 \times 100\ \% \quad (5)$$

where A_0 represented the initial wound area, and A_n represented the remaining area of wound treated by samples on day n (n = 1, 2, 3, 4, 5, 6).

12.3. Antibacterial Effect *In Vivo*

20 μL of the exudate collected from the wound site was diluted 1000 times with the LB medium. 100 μL of each dilution was evenly smeared on the LB agar plate at 37 °C for 24 h.

Spread plate images were captured by a digital camera. The antibacterial ratio was calculated utilizing the following equation:

$$\text{Antibacterial efficiency (\%)} = (N_C - N_T) / N_C \times 100\ \% \quad (6)$$

where N_C represented CFUs of the control group, and N_T represented CFUs of other treatment groups.

12.4. Histological Analysis

The tissue samples collected were immobilized in 4 % paraformaldehyde for 48 h, embedded by paraffin and cut into 6 μm sections. The tissue slides were stained by H&E (Sigma) and Masson's trichrome staining (Sigma) as the manufacturer's instructions. The images were captured *via* an optical microscope (DMI 4000, Leica, German) for the determination of epithelialization, angiogenesis, and collagen deposition. Subsequently, to assess the level of local inflammation responses, immunohistochemical staining for IL-1β and TNF-α were performed. Besides, immunofluorescence staining including VEGF and CD31 biomarkers was performed to evaluate the level of angiogenesis. The images were captured by CLSM. The collagen deposition, epithelium thickness and expression of fluorescence intensity were quantified using Image J software.

13. Statistical Analysis

Graphpad Prism 8.0 was used to calculate data and measure differences between groups using student *t*-test, one way and two-way ANOVA tests followed by a Tukey post hoc test for pairwise comparison. A value of $p \leq 0.05$ was considered statistically in the present study.

Reference

1. H. Zhao, J. Huang, Y. Li, X. Lv, H. Zhou, H. Wang, Y. Xu, C. Wang, J. Wang and Z. Liu, *Biomaterials*, 2020, **258**, 120286.

2. B. Tao, C. Lin, Z. Yuan, Y. He, M. Chen, K. Li, J. Hu, Y. Yang, Z. Xia and K. Cai, *Chemical Engineering Journal*, 2021, **403**.

3. X. Li, X. Huang, S. Xi, S. Miao, J. Ding, W. Cai, S. Liu, X. Yang, H. Yang, J. Gao, J. Wang, Y. Huang, T. Zhang and B. Liu, *Journal of the American Chemical Society*, 2018, **140**, 12469-12475.

4. L. Li, S. Cao, Z. Wu, R. Guo, L. Xie, L. Wang, Y. Tang, Q. Li, X. Luo, L. Ma, C. Cheng and L. Qiu, *Advanced Materials*, 2022, **34**, 2108646.

5. A. L. Z. Lee, V. W. L. Ng, G. L. Poon, X. Ke, J. L. Hedrick and Y. Y. Yang, *Advanced Healthcare Materials*, 2015, **4**, 385-394.

6. T. Jayaramudu, K. Varaprasad, R. D. Pyarasani, K. K. Reddy, A. Akbari-Fakhrabadi, V. Carrasco-Sánchez and J. Amalraj, *Carbohydrate Polymers*, 2021, **254**, 117302.

Captions of Figures

Figure S1. (a) EDS profile, (b) mapping of Bi_2S_3@GO nano-HJs.

Figure S2. (a) Maximum fracture force and (b) Young's modulus of a series of hydrogels, n = 3; Self-healing behavior of (c) Agar gel and (d) KC-Agar gel.

Figure S3. (a) Comparison of photothermal performances between Bi_2S_3@GO nano-HJs and photonic hydrogels upon 808 nm NIR laser irradiation; (b) The schematic diagram of heat dissipation in DN hydrogels; (c) Real-time infrared thermal images of Bi_2S_3@GO nano-HJs and photonic hydrogels. (P.S. : Real-time infrared thermal images of Bi_2S_3@GO nano-HJs in Figure S3c is same with that of BG 20:1 in Figure 3g, both of which are the same group and share original data.)

Figure S4. Photodynamic performance of KC-Agar gel: Reduction of DPBF for the detection of $^1O_2$ and $\cdot O_2^-$ in KC-Agar gel (a) without and (b) with 808 nm NIR irradiation (1.5 W/cm^2); ESR spectra of KC-Agar gel for (c) $^1O_2$ and (d) $\cdot O_2^-$ under 808 nm NIR irradiation.

Figure S5. Comparison of ROS generation of photonic hydrogels with NIR illumination under different quenching conditions (n = 3 independent experiments).

Figure S6. (a) UV-vis absorption spectrum of Bi_2S_3 nano-urchins, GO nano-sheets and Bi_2S_3@GO nano-HJs; (b) The bandgap and (c) the VB of Bi_2S_3@GO nano-HJs; (d) The schematic diagram of bandgap of Bi_2S_3@GO nano-HJs.

Figure S7. (a) The temperature curve over time, and (b) the L929 cells viability of control with NIR laser exposure dependent on time (0, 1, 2…15 min). n = 3; n.s.: no significant difference.

Figure S8. *In vitro* cytocompatibility of photonic hydrogels: Cell viability of Hacat cells treated with a series of hydrogels (a) in the dark and (b) upon 808 nm NIR laser irradiation (1.5 W/cm^2) for 15 min; (c) SEM images and (d) fluorescent images of Hacat cells cultured

on a series of hydrogels in the dark and upon 808 nm NIR laser irradiation (1.5 W/cm^2). n = 3; *p < 0.05; n.s.: no significant difference.

Figure S9. Cell viability of (a) L929 and (c) Hacat cells after treated with Bi_2S_3@GO nano-HJs upon 808 nm NIR laser irradiation (1.5 W/cm^2) for 15 min; Comparison of cell survival rate of (b) L929 and (d) Hacat cells after treated with Bi_2S_3, GO and Bi_2S_3@GO nano-HJs and photonic hydrogels under 808nm NIR laser illumination (1.5 W/cm^2). n = 3; *p < 0.05.

Figure S10. Results of wound scratch assays *in vitro*: (a) Images of wound closure at different time points such as 0, 12, and 60 h after treatment. Scale bar = 500 μm; (b) Migration rate of L929 cells around the wounds in different groups at 12 and 60 h. n = 3; *p < 0.05.

Figure S11. H&E staining images of heart, liver, spleen, lung, and kidney of mice from the different groups after 6 days treatment.

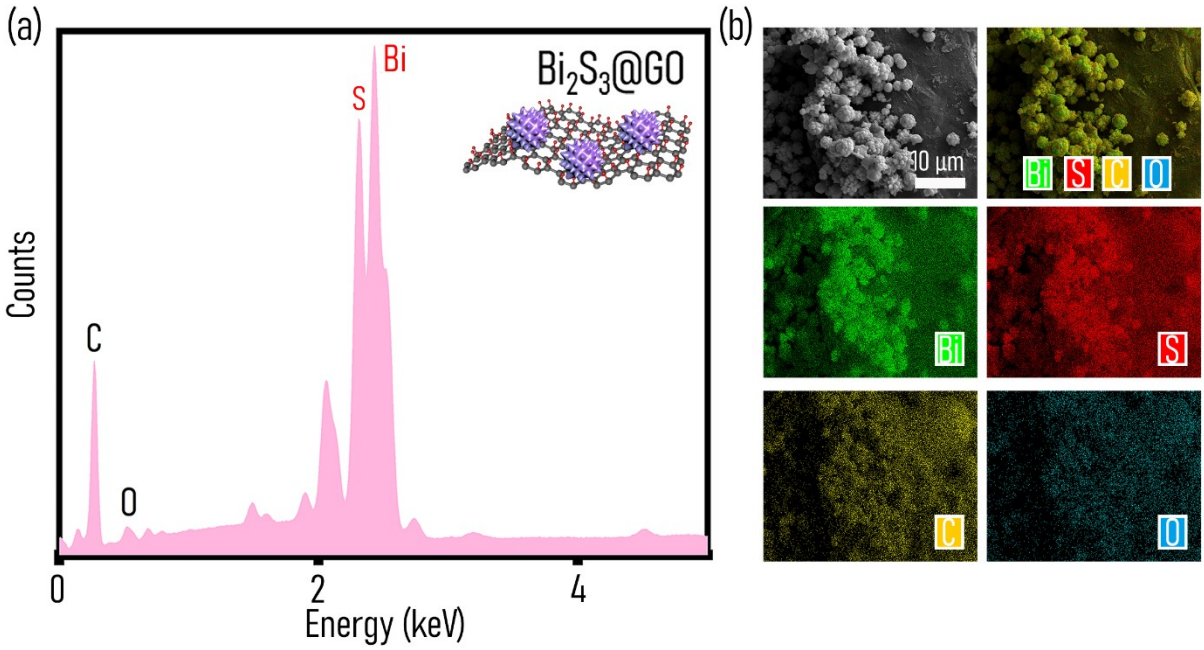

Figure S1. (a) EDS profile, (b) mapping of Bi_2S_3@GO nano-HJs.

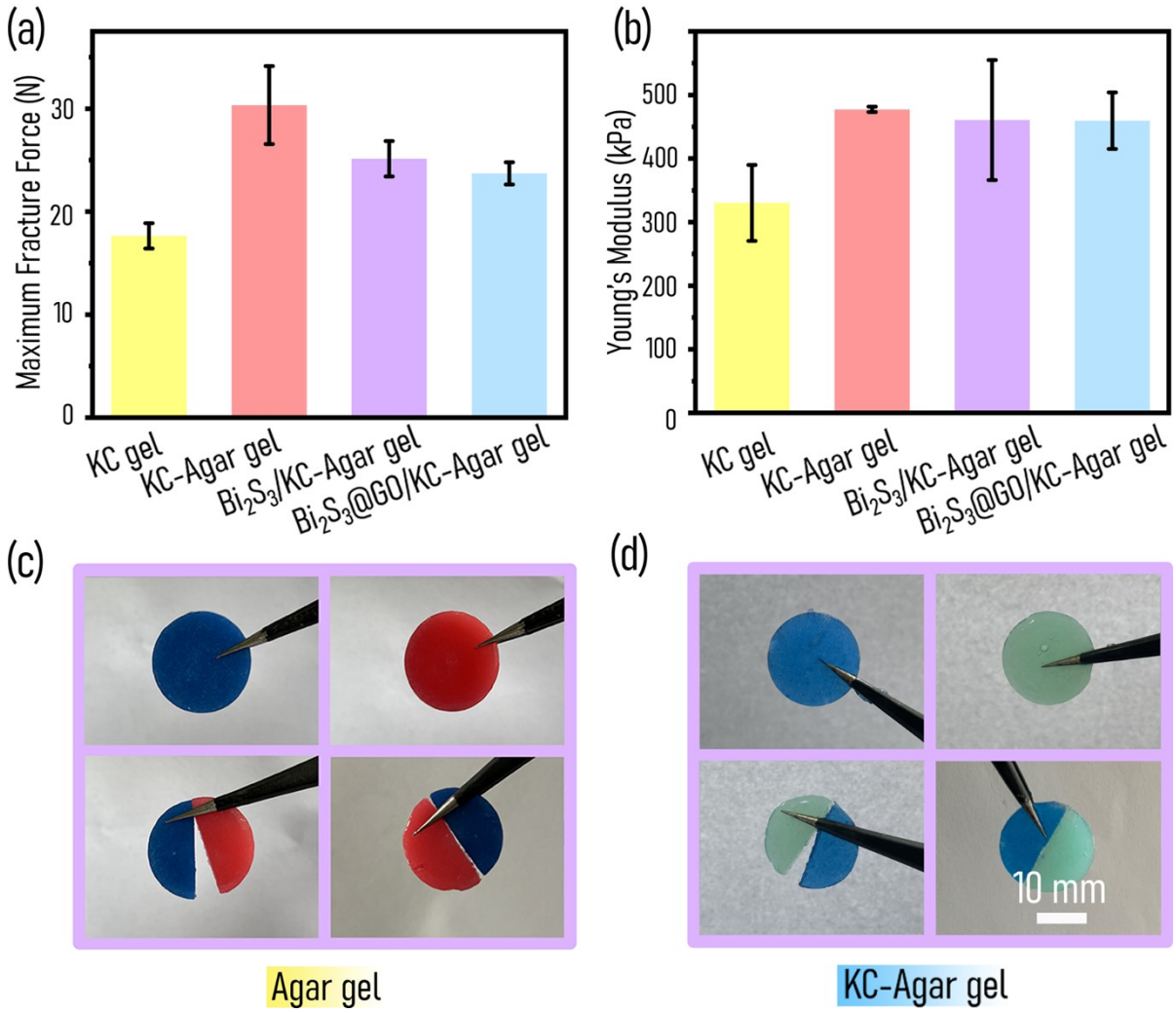

Figure S2. (a) Maximum fracture force and (b) Young's modulus of a series of hydrogels, n = 3; Self-healing behavior of (c) Agar gel and (d) KC-Agar gel.

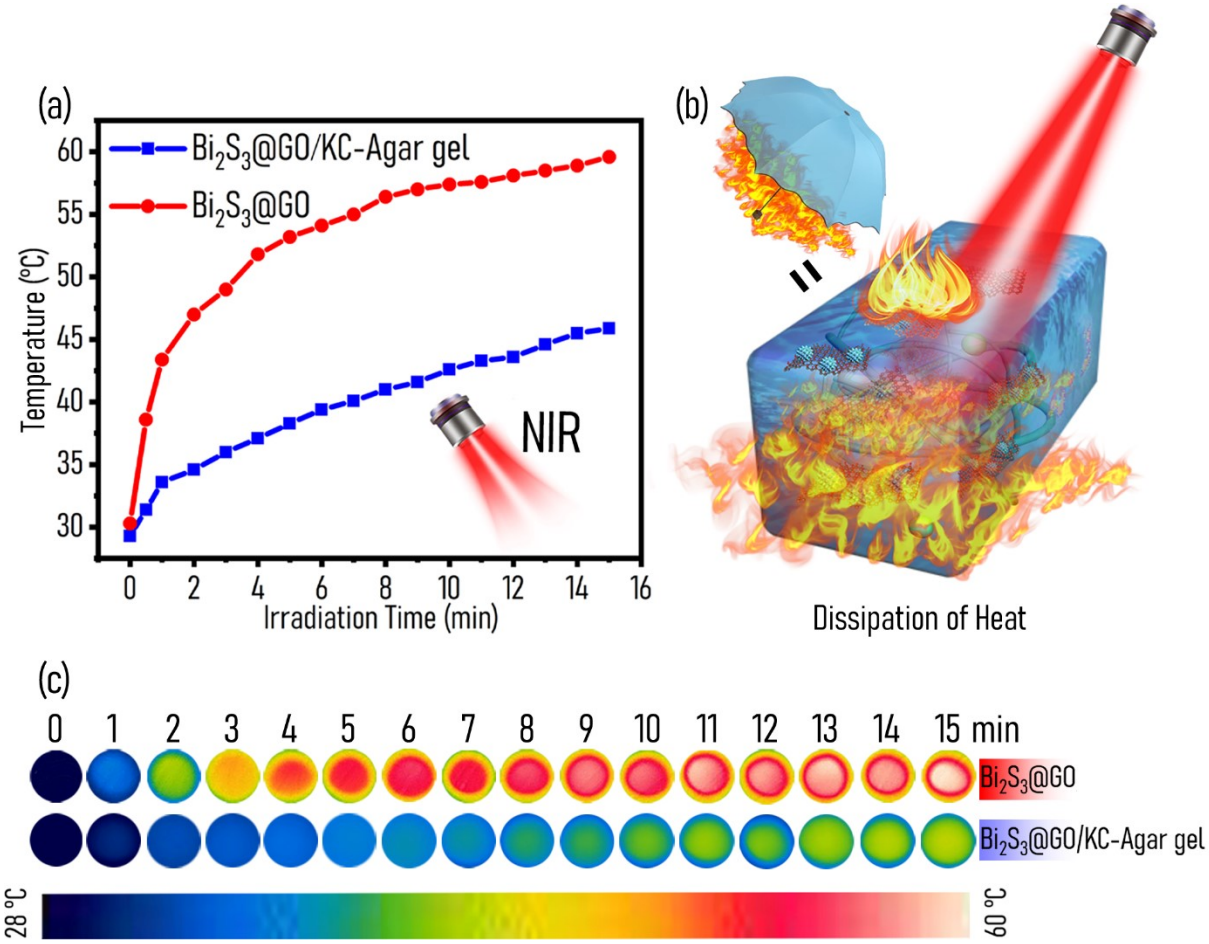

Figure S3. (a) Comparison of photothermal performances between Bi_2S_3@GO nano-HJs and photonic hydrogels upon 808 nm NIR laser irradiation; (b) The schematic diagram of heat dissipation in DN hydrogels; (c) Real-time infrared thermal images of Bi_2S_3@GO nano-HJs and photonic hydrogels. (P.S. : Real-time infrared thermal images of Bi_2S_3@GO nano-HJs in Figure S4c is same with that of BG 20:1 in Figure 3g, both of which are the same group and share original data.)

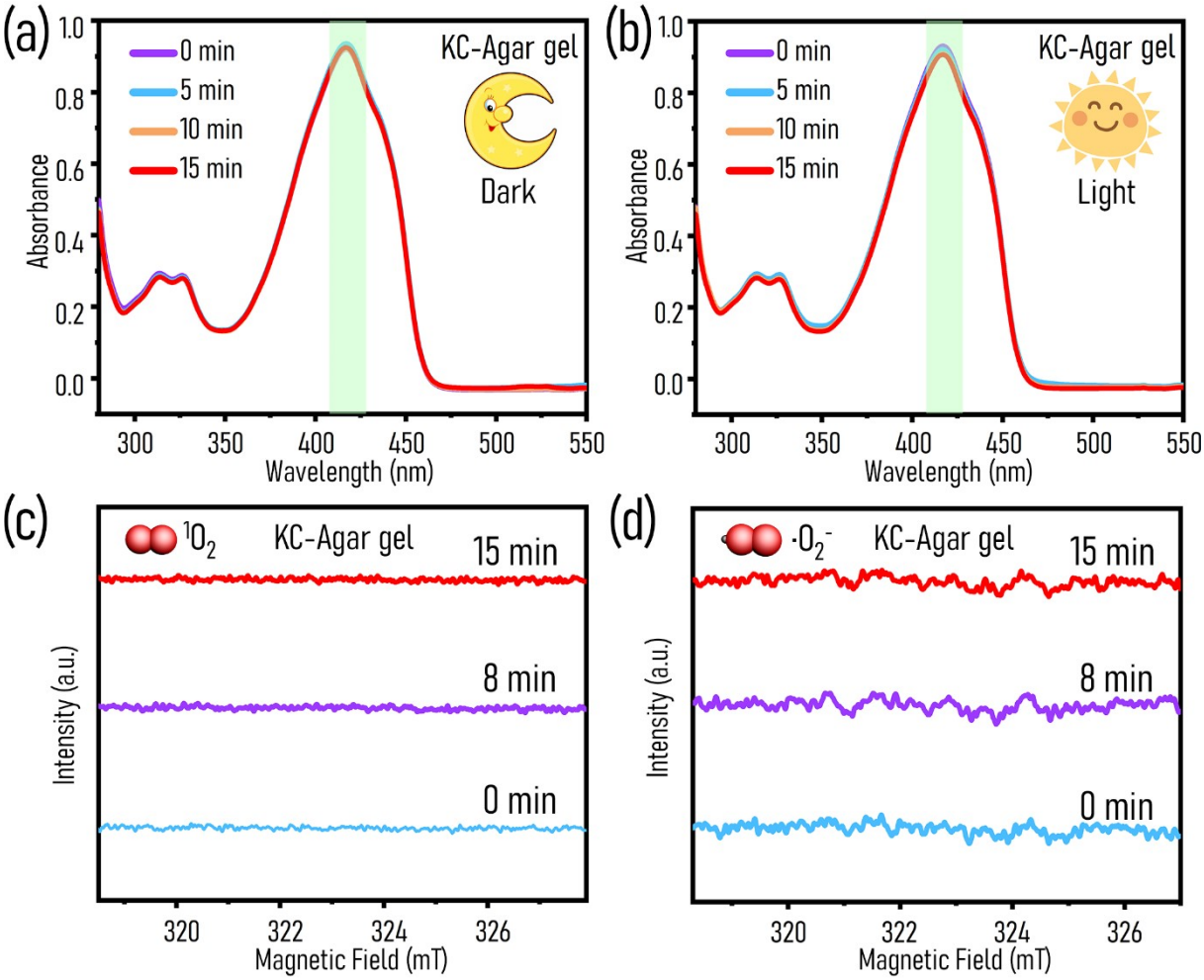

Figure S4. Photodynamic performance of KC-Agar gel: Reduction of DPBF for the detection of $^1O_2$ and $\cdot O_2^-$ in KC-Agar gel (a) without and (b) with 808 nm NIR irradiation (1.5 W/cm^2); ESR spectra of KC-Agar gel for (c) $^1O_2$ and (d) $\cdot O_2^-$ under 808 nm NIR irradiation.

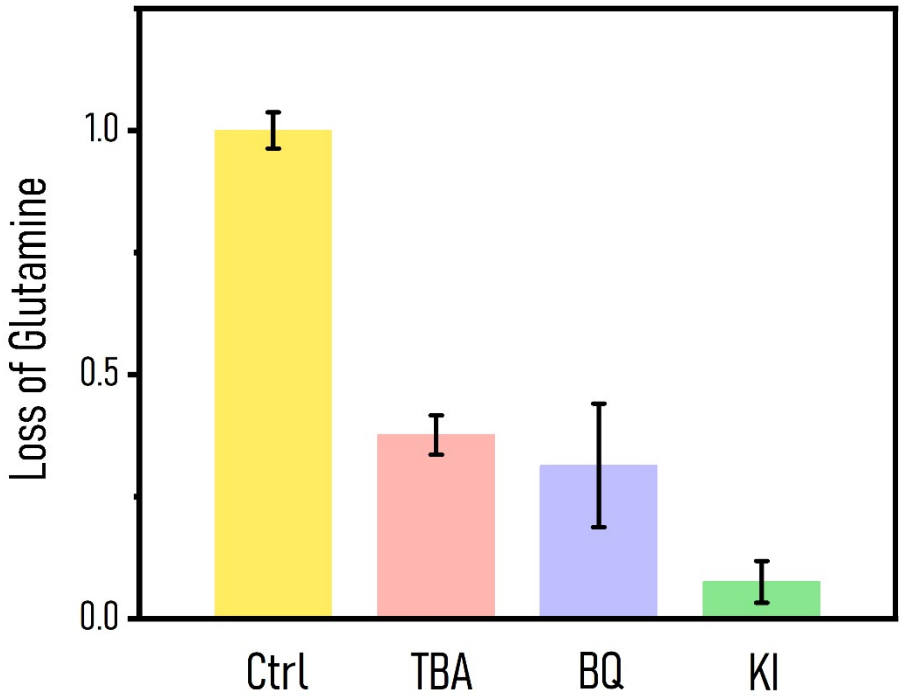

Figure S5. Comparison of ROS generation of photonic hydrogels with NIR illumination under different quenching conditions (n = 3 independent experiments).

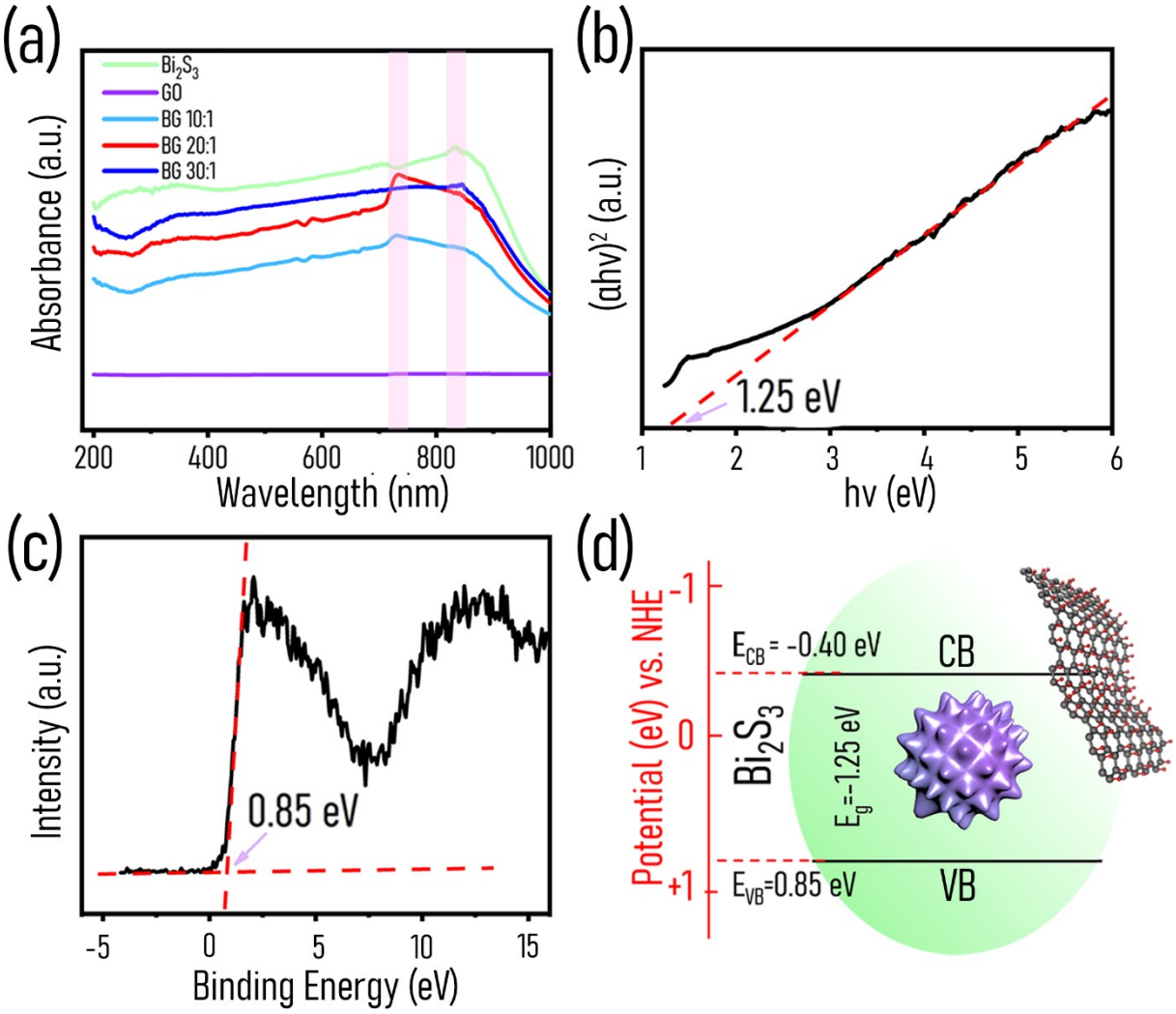

Figure S6. (a) UV-vis absorption spectrum of Bi_2S_3 nano-urchins, GO nano-sheets and Bi_2S_3@GO nano-HJs; (b) The bandgap and (c) the VB of Bi_2S_3@GO nano-HJs; (d) The schematic diagram of bandgap of Bi_2S_3@GO nano-HJs.

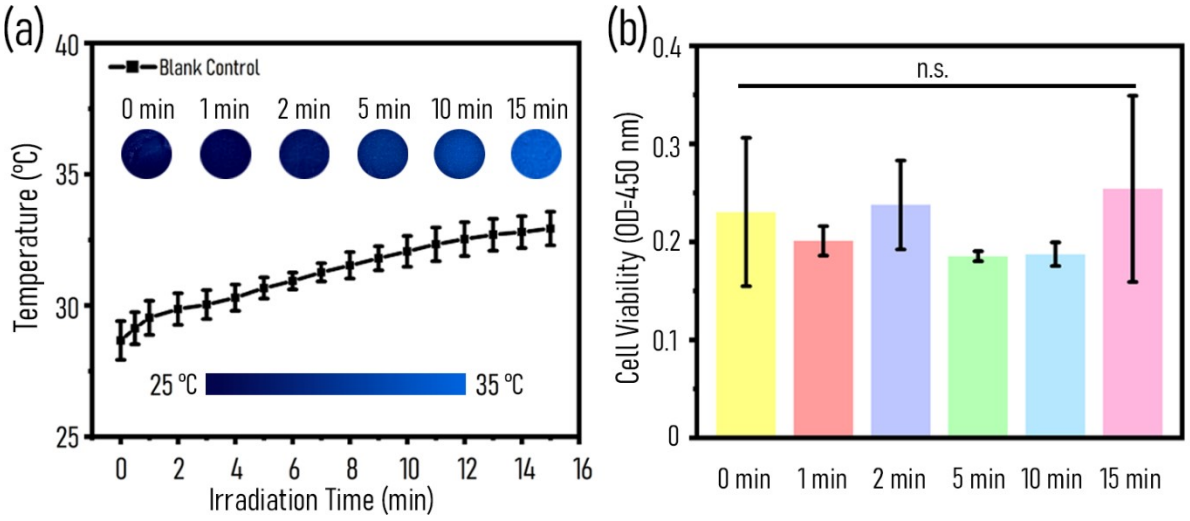

Figure S7. (a) The temperature curve over time, and (b) the L929 cells viability of control with NIR laser exposure dependent on time (0, 1, 2…15 min). n = 3; n.s.: no significant difference.

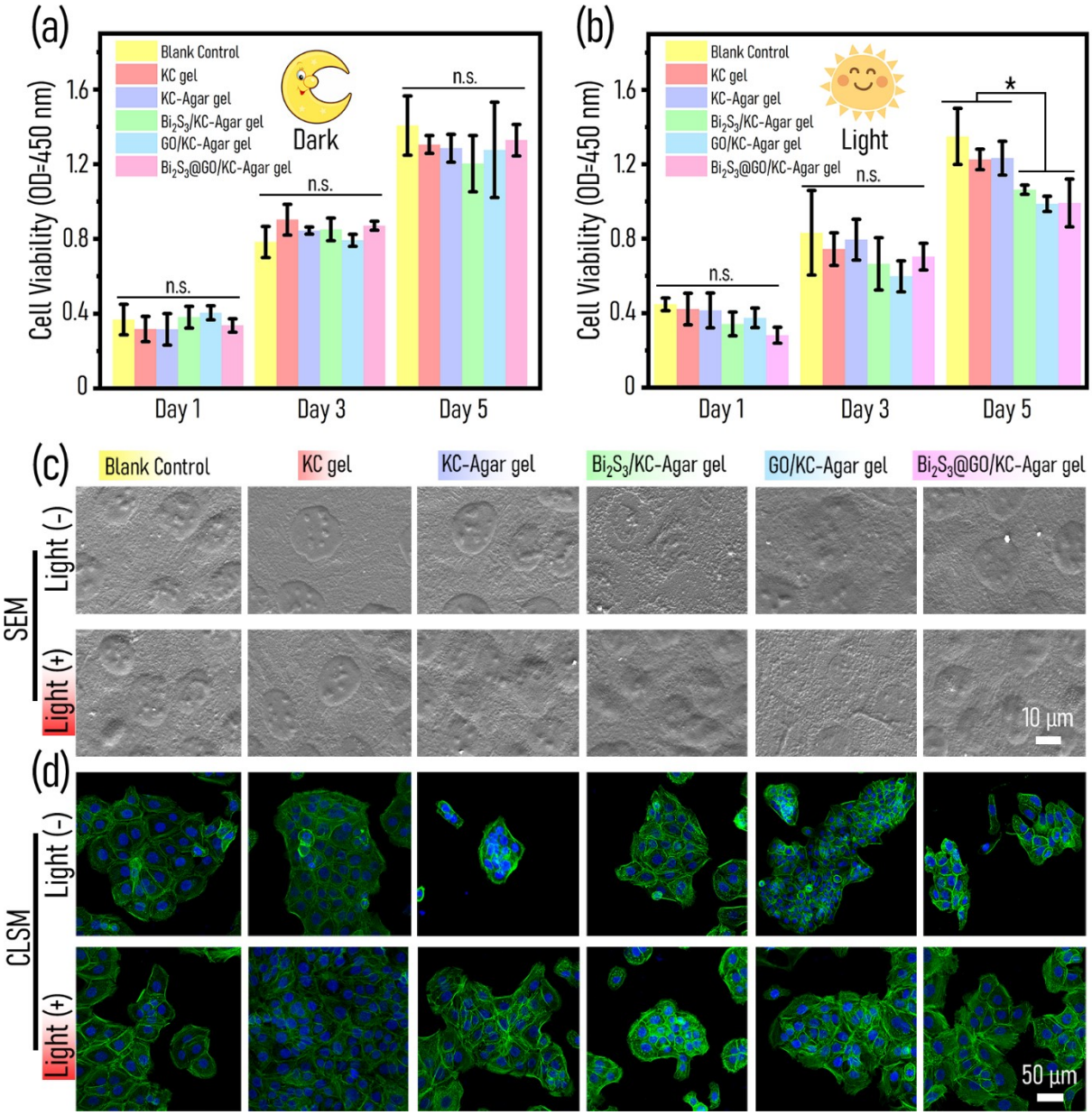

Figure S8. *In vitro* cytocompatibility of various photonic hydrogels: Cell viability of Hacat cells treated with a series of hydrogels (a) in the dark and (b) upon 808 nm NIR laser irradiation (1.5 W/cm^2) for 15 min; (c) SEM images and (d) fluorescent images of Hacat cells cultured on a series of hydrogels in the dark and upon 808 nm NIR laser irradiation (1.5 W/cm^2). n = 3; *$p < 0.05$; n.s.: no significant difference.

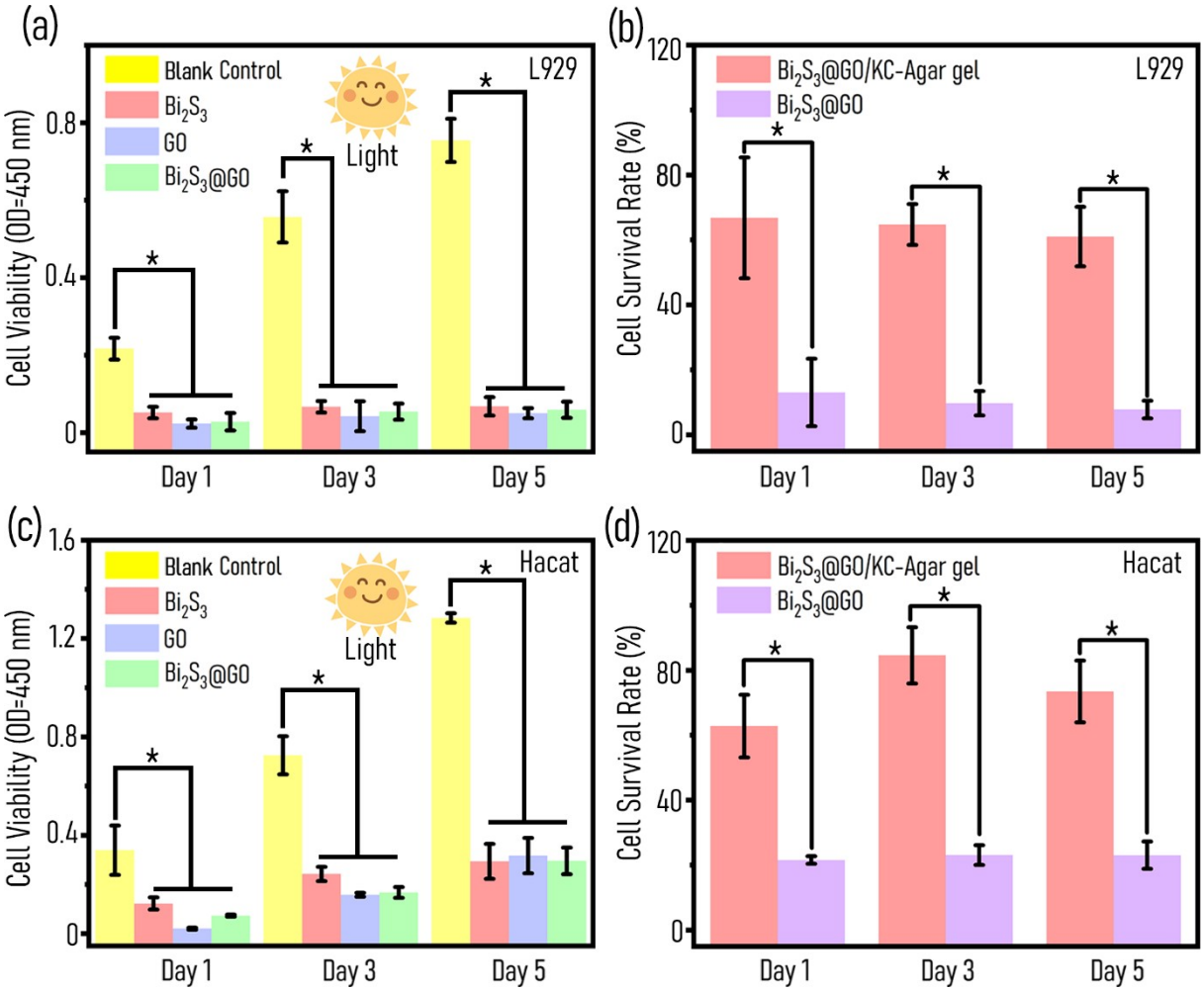

Figure S9. Cell viability of (a) L929 and (c) Hacat cells after treated with Bi_2S_3, GO, and Bi_2S_3@GO nano-HJs upon 808 nm NIR laser irradiation (1.5 W/cm^2) for 15 min; Comparison of cell survival rate of (b) L929 and (d) Hacat cells after treated with Bi_2S_3@GO nano-HJs and photonic hydrogels under 808nm NIR laser illumination (1.5 W/cm^2). n = 3; *$p < 0.05$.

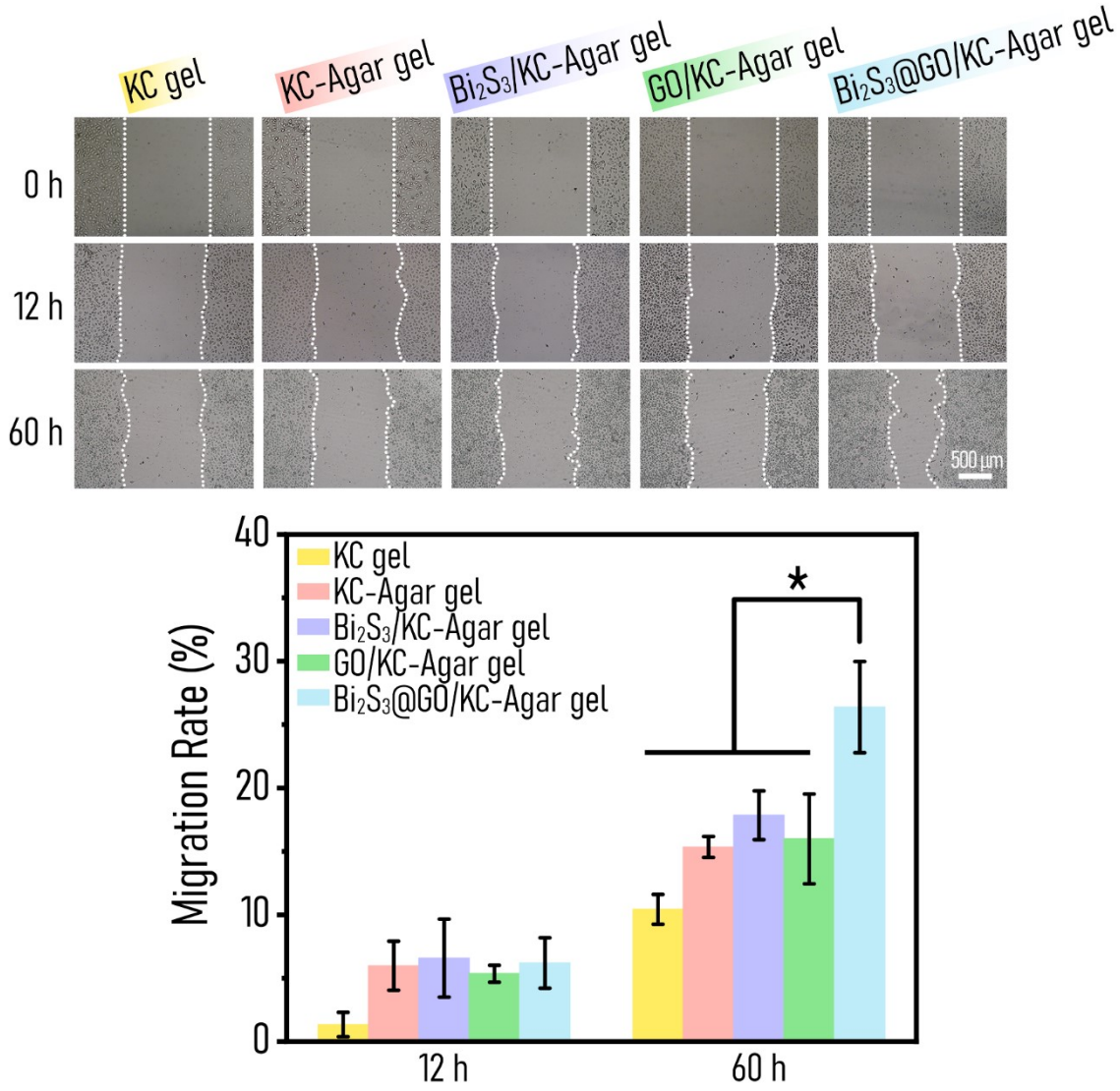

Figure S10. Results of wound scratch assays *in vitro*: (a) Images of wound closure at different time points such as 0, 12, and 60 h after treatment. Scale bar = 500 μm; (b) Migration rate of L929 cells around the wounds in different groups at 12 and 60 h. n = 3; *p < 0.05.

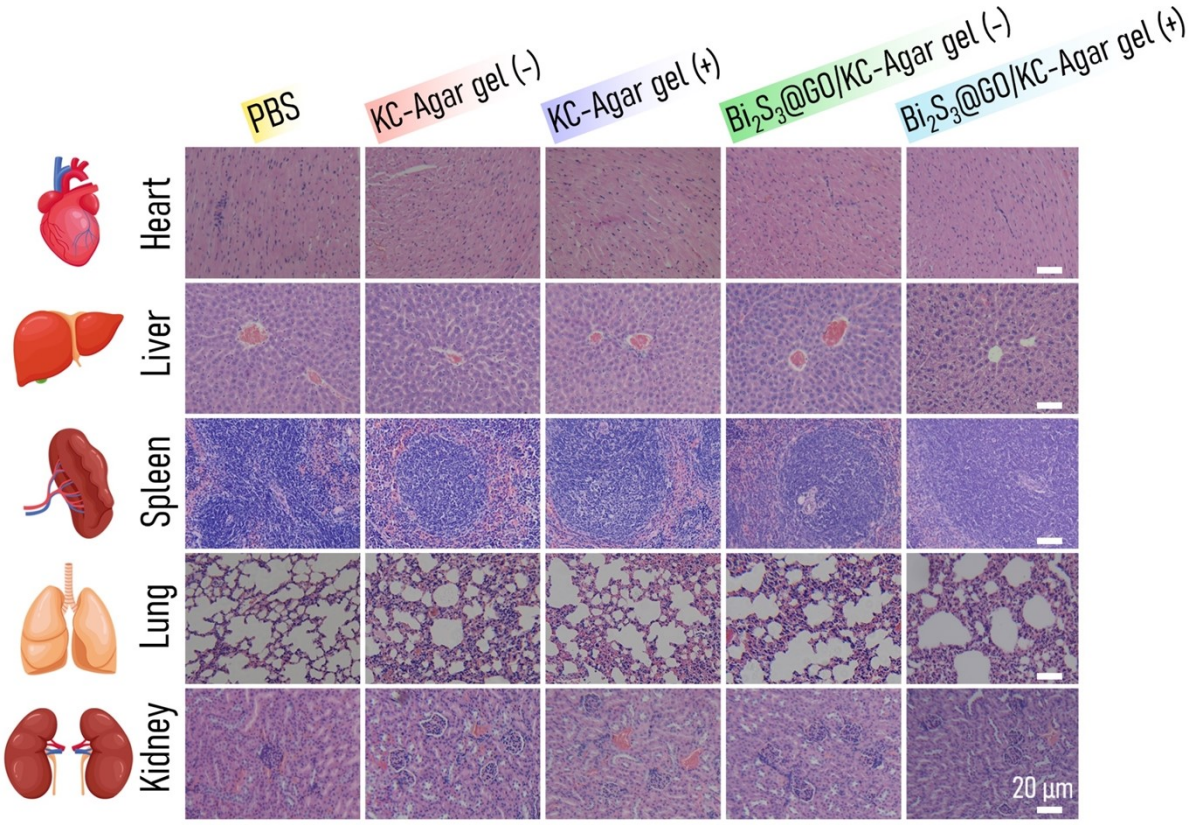

Figure S11. H&E staining images of heart, liver, spleen, lung, and kidney of mice from the different groups after 6 days treatment.

Table S1. MIC and MBC of Bi_2S_3 in the gel under 808 nm NIR irradiation for 15 min

Strains	**MIC (μg/mL)**	**MBC (μg/mL)**
	Bi_2S_3	**Bi_2S_3**
S. aureus	1600	3200
E. coli	1600	3200